



# Friction characterization and compensation in electro-mechanical systems

Tegoeh Tjahjowidodo<sup>a,\*</sup>, Farid Al-Bender<sup>b</sup>, Hendrik Van Brussel<sup>b</sup>, Wim Symens<sup>a</sup>

<sup>a</sup>*Flanders' Mechatronics Technology Centre, Celestijnenlaan 300D, B3001 Heverlee, Belgium*

<sup>b</sup>*Mechanical Engineering Department, Division PMA, Katholieke Universiteit Leuven, Celestijnenlaan 300B, B3001 Heverlee, Belgium*

Accepted 21 March 2007

The paper review of this article was organised by the Guest Editor.

---

## Abstract

Friction characterization is a prerequisite for an accurate control of electromechanical systems. This paper considers the identification and control of friction in a high load torque DC motor to the end of achieving accurate tracking. In the first place, model-based feedforward controllers for friction compensation are considered. For this purpose, friction model structures ranging from the classical Coulomb model through the recently developed generalized Maxwell slip (GMS) model are employed. The performance of those models is compared and contrasted in regard both to identification and to compensation. Subsequently, having an accurate model of the system, model-based feedback controllers are also considered, namely the DNPF and the gain scheduling controllers. We show further that the gain scheduling controller yields best performance.

© 2007 Elsevier Ltd. All rights reserved.

---

## 1. Introduction

In high precision positioning applications, the effects of friction present in the system can lead to significant positioning error. In order to compensate the error due to frictional forces, an effective control strategy is a prerequisite. As a consequence of the complex behaviour of friction, linear control strategies are generally unsuitable for providing an optimal performance for controlling a motion of systems with friction. Proportional-derivative (PD) and proportional-integrative-derivative (PID) actions are the most common in industrial applications. Introducing an integrative action in the controller may minimize the steady state error of the system, however, this action results in a slower response of the system and might lead to a limit cycle problem [1]. On other hand, as mentioned also in [1], without integrative action, a PD controller may exhibit higher steady state error, even though increasing the derivative (D) gain can eliminate the stick-slip problem due to increasing damping in the system.

If an accurate model of the system is available, a compensation of the error in the system can be made by applying a feedforward command that is equal to and opposite to the instantaneous force. The strategy of this

---

\*Corresponding author. Tel.: +32 16 328041; fax: +32 16 328064.  
E-mail address: [tegoeh.tjahjowidodo@fimt.be](mailto:tegoeh.tjahjowidodo@fimt.be) (T. Tjahjowidodo).

model-based compensation actually can be made by using a measured state as input to the model of the system, which makes the system compensated in feedback loop. However, the use of the desired input is more common in industrial applications [2].

A simple (although incomplete) representation of friction, i.e. classical approximation of Coulomb friction model, is sometimes adequate for the analysis of many practical systems. However, the Coulomb model defines the friction force only for non-zero relative velocity,  $v$ , in the sliding regime ( $v \neq 0$ ); when  $v = 0$  the characteristic simply sets the friction force below the static force value. In fact, however, motion never starts or stops abruptly and micro-sliding displacements are actually observed [3,4].

Two different friction regimes have been distinguished in the literature: the pre-sliding regime, where the friction force appears predominantly as a function of displacement [4,5]; and the sliding regime, where the friction force is predominantly a function of sliding velocity [3,6]. The pre-sliding regime is taken into account in some advanced models, such as LuGre [7], the Leuven and the most recent Generalized maxwell-slip (GMS) models [8].

Extending the method of linear feedback controller, Southward et al. [9] modify the proportional gain in the PD controller by adding an extra compensation force when the position error, as a controller input, is within the sticking distance. Therefore, they utilize a nonlinear proportional controller, in which they call the control strategy: discontinuous nonlinear proportional feedback (DNPF). A similar idea has also been proposed by Cai and Song [10] introducing another approach which they call the smooth robust nonlinear feedback (SRNF). This controller uses a nonlinear addendum to supplement an existing PD scheme. The additive force to the controller utilizes a sigmoid-like function of the position error. Extensive studies of the application of these techniques can be found in some papers (see e.g. Refs. [1,11]). These two controller approaches utilize only minimum knowledge of friction in the system. They only use static friction and pre-sliding (stiction) distance to implement those techniques and no further information is required.

Al-Bender and Symens [12] proposed the idea of a gain scheduling controller technique based on the equivalent dynamic properties, namely stiffness and damping, which are evaluated utilizing a describing function (DF) technique for a mass subjected to hysteretic frictional element. The controller they proposed consists of two main control modes. The first mode is dealing with the gross-sliding friction where the system uses a linear compensation scheme together with equivalent Coulomb friction compensation. When the motion is reversed and when the distance to the desired position is within the pre-sliding limit, a second mode of the controller is activated until the motion leaves the pre-sliding region again. In this mode, the controller uses scheduled gains, which are designed based on the equivalent dynamic properties of the system.

The objective of this paper is to characterize frictional behaviour in an electro-mechanical system, more specifically, to use this knowledge to design effective control schemes. Various friction models are first outlined and evaluated by application in feedforward compensation schemes. Afterwards, some nonlinear feedback control strategies, including a gain scheduling controller utilizing the knowledge obtained from identification are implemented for friction compensation.

In the following, Section 2 formulates the DC motor torque balance, and outlines the friction models used in this investigation. Section 3 describes the experimental apparatus, while Section 4 discusses the friction identification procedure. Thereafter, the model-based feedforward friction compensation scheme is sketched in Section 5. Section 6 presents some results utilizing various types of nonlinear control schemes, while Section 7 presents the compensation results utilizing various nonlinear controllers. Finally, appropriate conclusions are drawn in Section 8.

## 2. Motor torques and friction models

In general, a DC motor can be viewed as a black box with two inputs: current and load torque, and one output angular displacement (or velocity). Torque balance for a DC motor can be written as

$$\tau_m = \tau_i + \tau_f + \tau_0, \quad (1)$$

where  $\tau_m$  is the motor torque generated by the amplifier current,  $\tau_i$  is the inertial torque from motor armature and shaft,  $\tau_f$  is the friction torque and  $\tau_0$  is the load torque.

As for the friction torque  $\tau_f$  in Eq. (1), which is our main concern, several models exist as described below.

### 2.1. Coulomb friction

The classical Coulomb model of friction is described by a discontinuous relation between the friction force and the relative velocity between the rubbing surfaces. In this model, when the mass that is subjected to friction is slipping, the friction force will remain constant until the motion is reversed.

### 2.2. Coulomb with Stribeck friction

The Stribeck friction consists of (i) a function  $s(v)$  that is decreasing in the velocity and bounded by an upper limit at zero velocity equal to the static friction force  $F_S$ , and a lower limit equal to the Coulomb force  $F_C$ , and (ii) a viscous friction part. In this approach, the constant portion of the Coulomb model is replaced by Stribeck function. In order to overcome the jump discontinuity of the Coulomb model, at  $v = 0$ , that jump is replaced by a line of finite slope, up to a very small threshold  $\varepsilon$ , as shown in Fig. 1. Mathematically, the function can be represented as follows:

$$F = \begin{cases} F_C + (F_S - F_C)e^{|v/V_S|^\delta}, & |v| > \varepsilon, \\ (v/\varepsilon)[F_C + (F_S - F_C)e^{|v/V_S|^\delta}], & |v| \leq \varepsilon, \end{cases}$$

where  $F_C$  represents the Coulomb friction force at zero velocity,  $F_S$  is the static friction force,  $V_S$  is the Stribeck velocity and  $\delta$  is the shaping factor of the Stribeck function, while  $\varepsilon$  is the threshold.

### 2.3. LuGre and Leuven models

The previous two methods are impractical for friction compensation at motion stop and inversion, where the worst effects due to friction, namely stick–slip motion, could arise. The LuGre model [7] was the first formulation that could effect a smooth transition between those two regimes, i.e. without recourse to switching functions. It, furthermore, accounts for other friction characteristics such as the breakaway force and its dynamics. The model achieves this by introducing a state variable, representing the average deflection of elastic bristles (representing surface asperities) under the action of a tangential force, together with a state equation, governing this variable's dynamics and friction equation.

However, this model has been subjected to important criticism [5] in regard to its failure to model pre-sliding/pre-rolling hysteresis with non-local memory. In this regime, the friction force shows hysteresis behaviour with non-local memory in that regime [4,5]. The latter authors proposed an extension in the form now known as the Leuven model and a subsequent improvement [13] to better facilitate the implementation of non-local memory hysteresis.

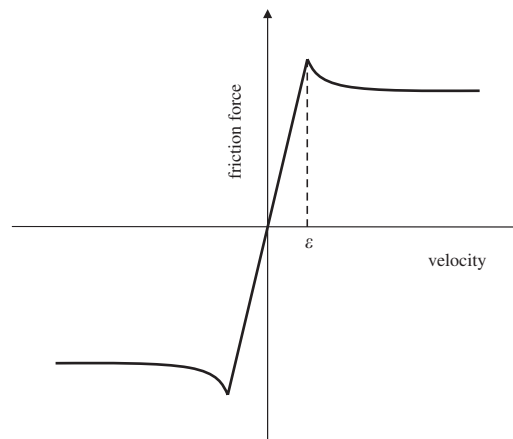


Fig. 1. Friction curve of Stribeck models.

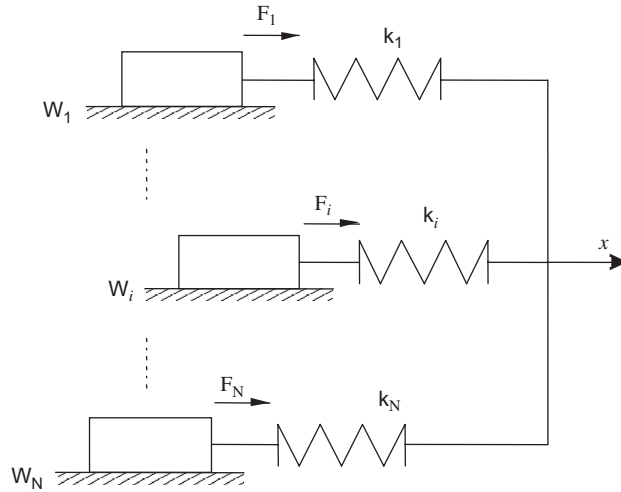


Fig. 2. Parallel connection of elementary state models of friction.

#### 2.4. GMS friction

The GMS friction model [6,14] is a qualitatively new formulation of the rate-state approach applied to the Maxwell-slip model [15]. The GMS model retains the (original) Maxwell-slip model structure, which is a parallel connection of different elementary slip-blocks and springs, but replaces the simple Coulomb law governing each block, by another state equation to account for sliding dynamics. Thus, the friction force is given as the summation of the outputs of the  $N$  elementary state models (see Fig. 2). The dynamic behaviour of each elementary block is represented by one of the two equations (in which  $F_i$  is the elementary friction force,  $k_i$  is the elementary spring constant, and  $v$  is the velocity):

- If the model is sticking:

$$\frac{dF_i}{dt} = k_i v. \quad (2)$$

- If the model is slipping:

$$\frac{dF_i}{dt} = \text{sgn}(v) C \left( \alpha_i + \frac{F_i}{s(v)} \right). \quad (3)$$

Each elementary model (or block) corresponds to a generalized asperity in the contact surface, where it can stick or slip. The asperity will slip if the elementary friction force equals the maximum value  $W_i = \alpha_i s(v)$  that it can sustain. In this regime, Eq. (3) will characterize the friction behaviour. Once the model is slipping, it remains slipping until the direction of movement is reversed or its velocity approaches zero value. When the asperity is sticking the elementary model will act as a spring with stiffness of  $k_i$ .

### 3. Experimental setup

Experimental identification and compensation of friction in a DC motor was performed on ABB motor type M19-S, with maximum rated torque of 0.49 Nm/A and armature inertia of 0.001 kgm<sup>2</sup>. Fig. 3 shows a schematic of the experimental setup. To allow a straightforward position and velocity data collection on the motor, an incremental angular encoder was connected to the shaft through a toothed belt and pulleys. The

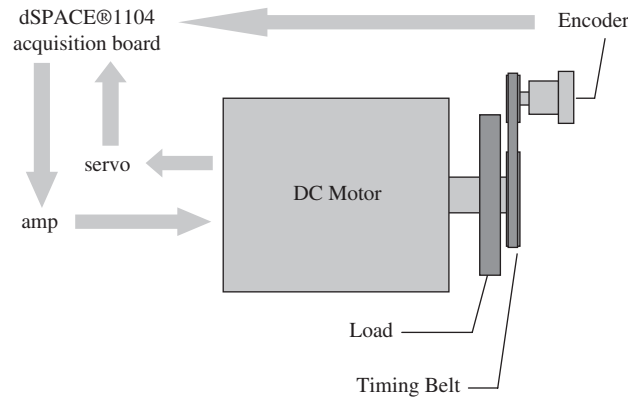


Fig. 3. Schematic of the setup.

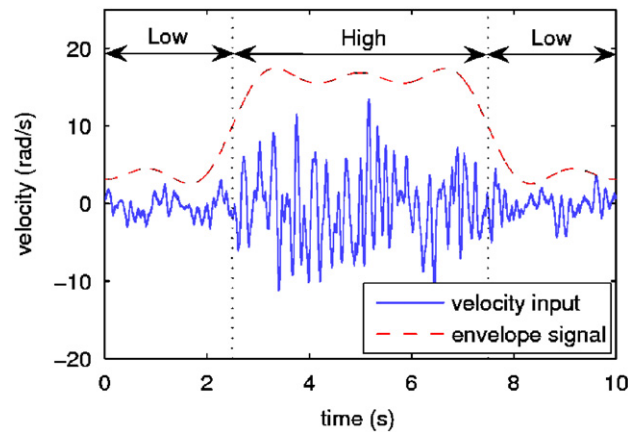


Fig. 4. Velocity input signal applied to the system for identification purpose. —, velocity input, - - - - -, envelope signal.

pulleys give a reduction ratio of 1:3 to increase the sensitivity of the encoder, whose resolution is 5000 pulses per revolution.

#### 4. Identification of friction

The identification experiment was carried out by applying an input velocity signal. A special input command was designed for this purpose. This command signal is composed of a band limited random signal with cut-off frequency of 4 Hz, which is enveloped by a certain signal. This envelope signal is composed of the three first non-zero terms of the Fourier series of a rectangular signal, which has period of 10 s. The purpose of enveloping the random signal is to emphasize the behaviour of pre-sliding friction in the experiment, which corresponds to the friction at low velocity and low displacement. The signal and its corresponding envelope are shown in Fig. 4. This signal was applied through a dSPACE-1104 acquisition card to the servo amplifier. The real current input to the motor, which is assumed to correspond to the torque was measured and recorded using the same acquisition unit.

Fifty thousand points, at 1 ms sampling time, were collected for each test. The first 10 s were used as a training set and the remaining 40 s were used as testing set. The Nelder–Mead Simplex algorithm was used for optimizing the parameters in each of the friction models and moment of inertia of the armature. The Nelder–Mead Simplex is a well-known heuristic search algorithm. The algorithm is stated using the term simplex (a generalized triangle in  $n$  dimensions) and will find the minimum of a function of  $n$  variables by

Table 1  
Performances of identification result for high frequencies experiment

	High velocity MSE (max. err.)	Low velocity MSE (max. err.)
Coulomb	4.00% (0.6757)	17.92% (1.2993)
Stribeck	0.55% (0.2762)	9.59% (1.2604)
LuGre	0.41% (0.2440)	4.30% (0.6466)
GMS <sub>4</sub>	0.40% (0.2350)	1.39% (0.5711)
GMS <sub>10</sub>	0.38% (0.2300)	1.19% (0.5177)

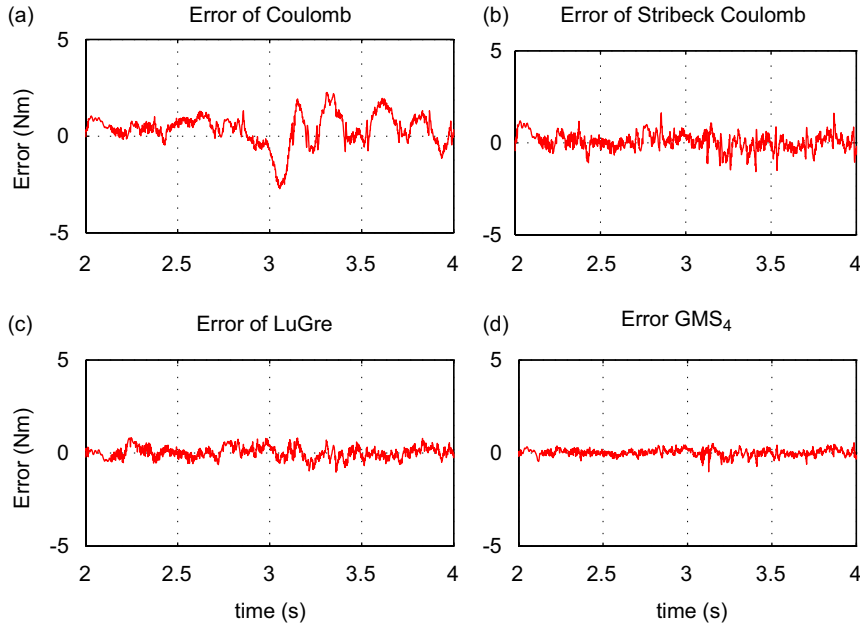


Fig. 5. Force Error of the estimated torques for various model-based compensation techniques: (a) error of Coulomb model, (b) error of Stribeck-Coulomb model, (c) error of LuGre model, (d) error of GMS model.

updating its vertex iteratively [16,17]. As a measure of performance, the normalized mean square error was used, which is defined by

$$MSE(\hat{y}) = \frac{100}{N\sigma_y^2} \sum_{i=1}^N (\hat{y}_i - y_i)^2, \tag{4}$$

where  $y$  is the output (in this case the experimentally measured friction force),  $\sigma_y^2$  is its variance and the caret denotes the estimated quantity of the friction force.

The performance values for each friction model can be found in Table 1. The values between brackets represent the peak-to-peak errors that are normalized by the RMS value of the actual torques. In this table the performances are divided into two groups, one for high velocities and the other for low velocities. Each group is calculated based on the envelope signal. High velocity performance values are calculated at the instances when the envelope velocity is high, while low velocity performance values are calculated when the envelope velocity is low.

The errors of the corresponding models are shown in Fig. 5, for Coulomb, Stribeck–Coulomb, LuGre and GMS (with four elements), from left to right and top to bottom, respectively. It can be seen that the identification results of the classical friction models fall far from the actual value in some regions. In the figure,

the error between 2 and 3 s corresponds to the low velocity regions (i.e. more pre-sliding regime portion, while between 3 and 4 s the velocity input is in the high region, see Fig. 5).

On the other hand, the results of the two recent models, LuGre and GMS, show much better performance. They give significant improvements, especially in the low velocity region, for which the classical models could not account well.

The most recent friction model, GMS, gives the best results in this experiment. In particular, strong improvement is achieved in the low velocity region. The ability to estimate the friction behaviour in pre-sliding regime is shown as the superiority of the GMS model, while it does not lose its ability to estimate the friction in the gross sliding regime.

As a comparison, another identification utilizing GMS model with a higher number of Maxwell-slip elements was conducted. In this identification, 10 Maxwell-slip elements were used, instead of four. Although this gives a slightly better result, the improvement is not significant as shown in the last row of Table 1. Increasing the Maxwell-slip by six elements means adding twice times six (= 12) parameters in the optimization process, which is a high price for the slight improvement.

In addition, the moment of inertia of the armature obtained from these identifications deviates slightly, less than 10% of the nominal value, 0.0012 kgm<sup>2</sup>.

## 5. Model-based feedforward friction compensation

In this section, position control incorporating friction compensation using the aforementioned models in the feedforward will be described. For this purpose, the inertial force and the friction force, as both are modelled in the previous section, are included in the feedforward loop. The control scheme is depicted in Fig. 6.

The feedback loop, which is required to track set-point changes and to suppress unmeasured disturbances, is chosen to be a PID controller with gains  $K_p = 200$  N m/rad,  $K_i = 0$  N m/rad s, and  $K_d = 0.15$  N m s/rad. In order to obtain a consistent comparison, these gains were optimized for one of the control schemes, namely that employing LuGre compensation, and used with the same values for all the other models. As a numerical quantification of the validation criterion, the root-mean-square tracking error is used for different reference input signals.

Two different reference signals were employed to validate the friction compensation. The first reference position signal is a filtered random signal with a very small stroke in order to emphasize the pre-sliding regime of the friction torque. The reference signal was generated using a random signal generator, which is driven through a low pass, fourth order digital Butterworth filter with 1 Hz cut-off frequency. The tracking error of each friction compensation model can be seen in Fig. 7. (All these results were obtained with the same PID controller parameters.) The numerical RMS values are given in Table 2.

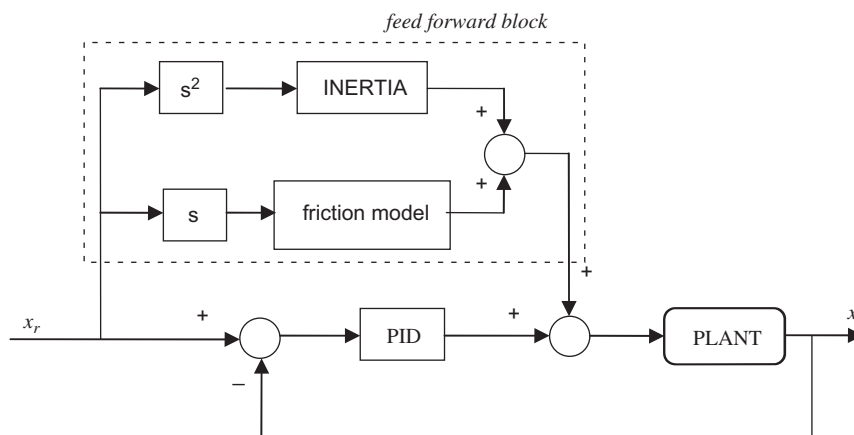


Fig. 6. The feedforward/feedback control scheme for friction compensation.

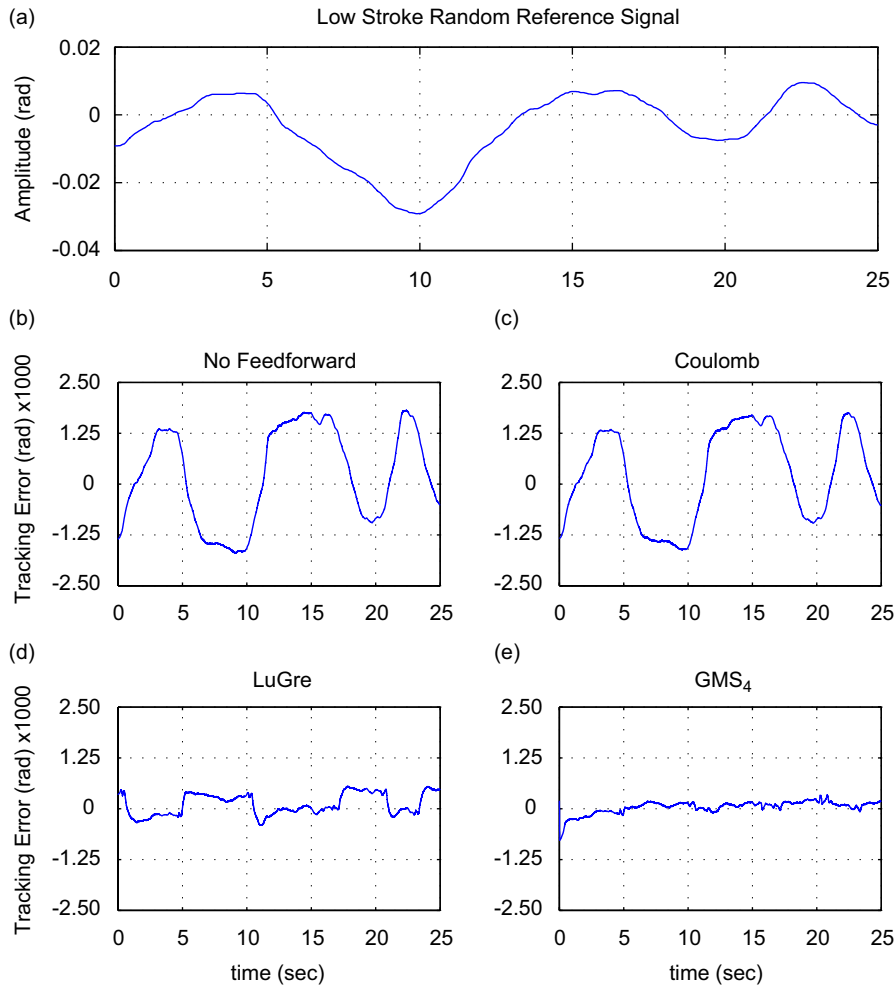


Fig. 7. The tracking errors for low stroke filtered random reference input: (a) the reference signal to the system, (b) the tracking error for a system with no feedforward friction compensation, (c) the tracking error for a system with Coulomb feedforward friction compensation, (d) the tracking error for a system with LuGre feedforward friction compensation, (e) the tracking error for a system with four-elements-GMS feedforward friction compensation.

Table 2  
Performances of friction compensation for a low stroke random input

Compensation	RMS ( $\text{rad} \times 1000$ )
No feedforward	1.20
Coulomb	1.10
LuGre	0.34
GMS	0.13

Friction compensation based on the Coulomb model yields large errors, and is almost identical to the scheme that has no feedforward compensation. Since the reference signal has a very small stroke and it is emphasizing the pre-sliding regime, the Coulomb model is merely playing on its threshold region. Thus, the Coulomb model will act only as a gain to the reference signal. The GMS model compensation, in contrast, gives significant improvement in comparison with the other models. It shows superiority at the reversal points compared to the LuGre model. The jumps in the tracking error of the LuGre model, which correspond to the sticking problem, are significantly reduced in the GMS compensation model.

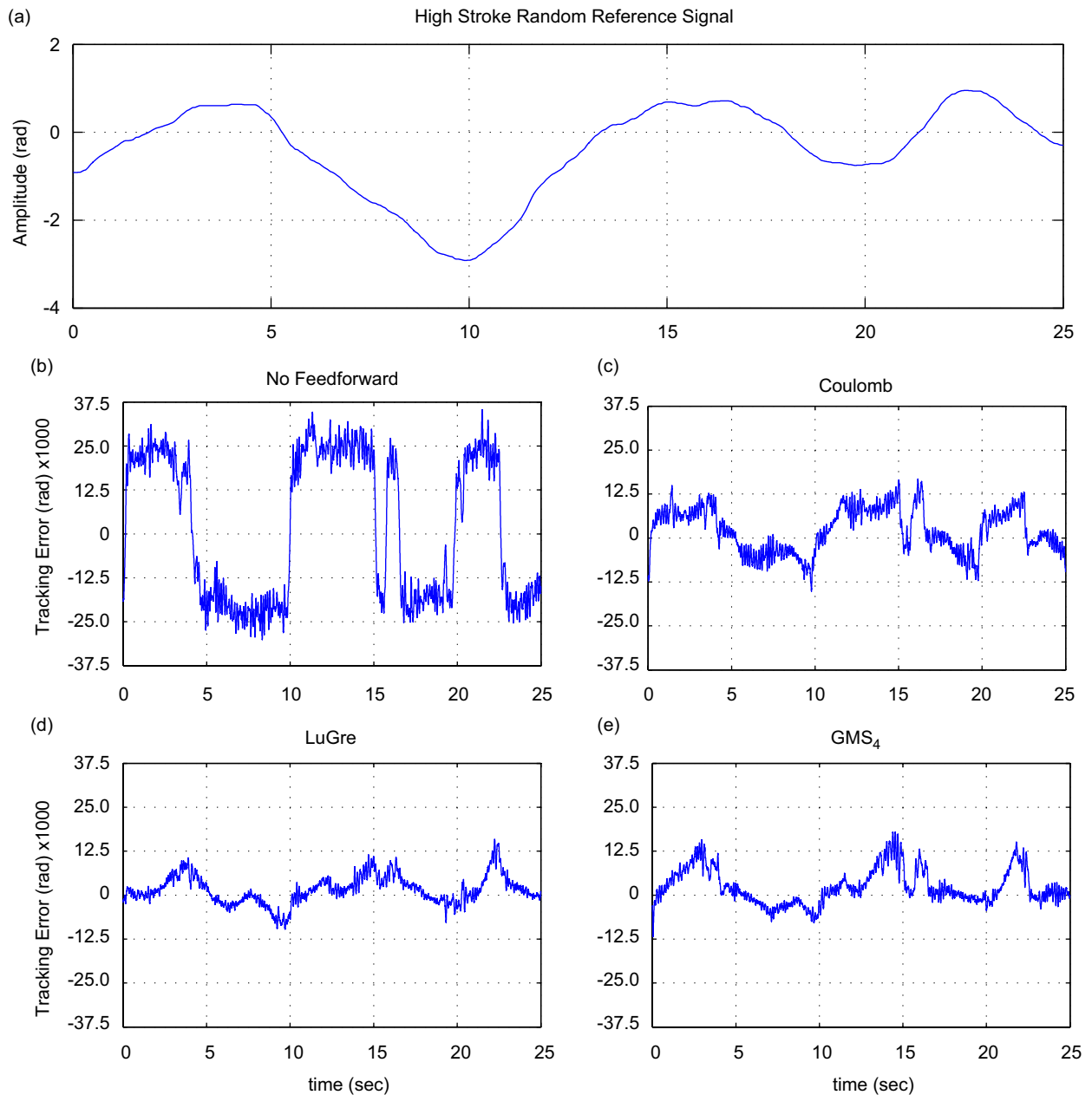


Fig. 8. The tracking errors for high stroke filtered random reference input: (a) the reference signal to the system, (b) the tracking error for a system with no feedforward friction compensation, (c) the tracking error for a system with Coulomb feedforward friction compensation, (d) the tracking error for a system with LuGre feedforward friction compensation, (e) the tracking error for a system with four-elements-GMS feedforward friction compensation.

The second reference signal used in this experiment is a filtered random signal similar to the signal in the previous experiment, except that this signal has larger amplitude. The maximum stroke of this random signal was set to  $\pi$  rad (or half of the shaft's rotation). In this case, the pre-sliding friction is not expected to dominate the overall behaviour.

The tracking errors for each compensation scheme are depicted in Fig. 8. For this desired position signal, the GMS model again gives the best performance. However, according to the performance values in Table 3, it does not give a significant improvement compared to the LuGre model, or for that matter, even the Coulomb

Table 3  
Performances of friction compensation for a high stroke random input

Compensation	RMS ( $10^{-3}$ rad)
No feedforward	21.1
Coulomb	11.5
LuGre	9.40
GMS	9.20

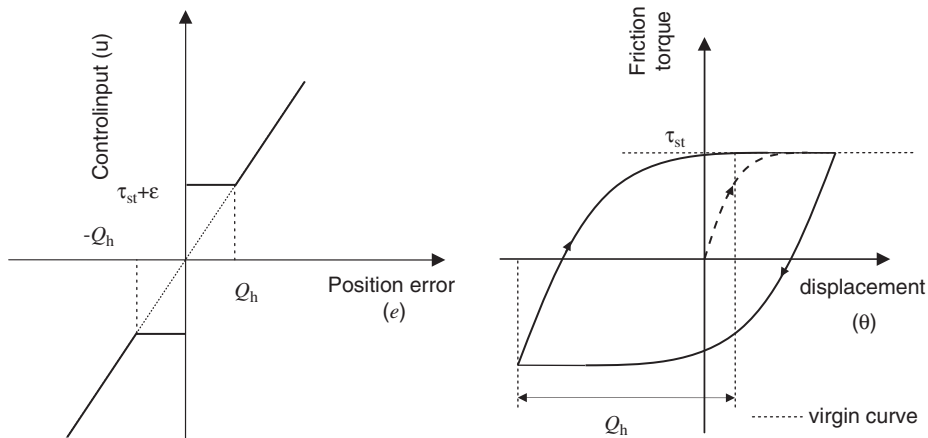


Fig. 9. The control input of the DPNF Controller. - - - -, virgin curve.

model: the maximum difference is 20%. These results are understandable, since the system was excited with a high stroke, i.e. more in sliding regime than in pre-sliding regime. In this case, the zero crossings of the velocity, where the pre-sliding regime friction arises, will occur only over a very short portion during the whole motion.

## 6. Nonlinear controller

The previous section considered the use of the different friction models in the feedforward loop of a conventional linear controller. This section will present two nonlinear controllers (without feedforward), designed on the basis of the Coulomb and the Maxwell-slip models, respectively.

### 6.1. Discontinuous nonlinear proportional feedback

The DPNF controller [9] adds an extra compensating torque, which is slightly higher than the Coulomb force,  $\tau_{st}$ , when the position error is small enough to lie within the pre-sliding region,  $Q_h$  (see Fig. 9). It uses the limits of the pre-sliding regime friction to provide bounds within which extra compensating control effort will be added.

Based on the previous identification step, we obtain a pre-sliding distance,  $Q_h$ , which is approximately equal to 0.004 rad corresponding to a static friction torque of 0.95 N m. The proportional gain in this controller is chosen in such a way that the friction compensation at zero velocity exceeds the static friction torque,  $u|_{v=0} = \tau_{st} + \epsilon$ .

### 6.2. Gain scheduling

The general idea of a gain scheduling controller is to adjust the controller gains based on the varying dynamic parameter of the system. Al-Bender et al. [18] formulated the equivalent dynamic parameters of the

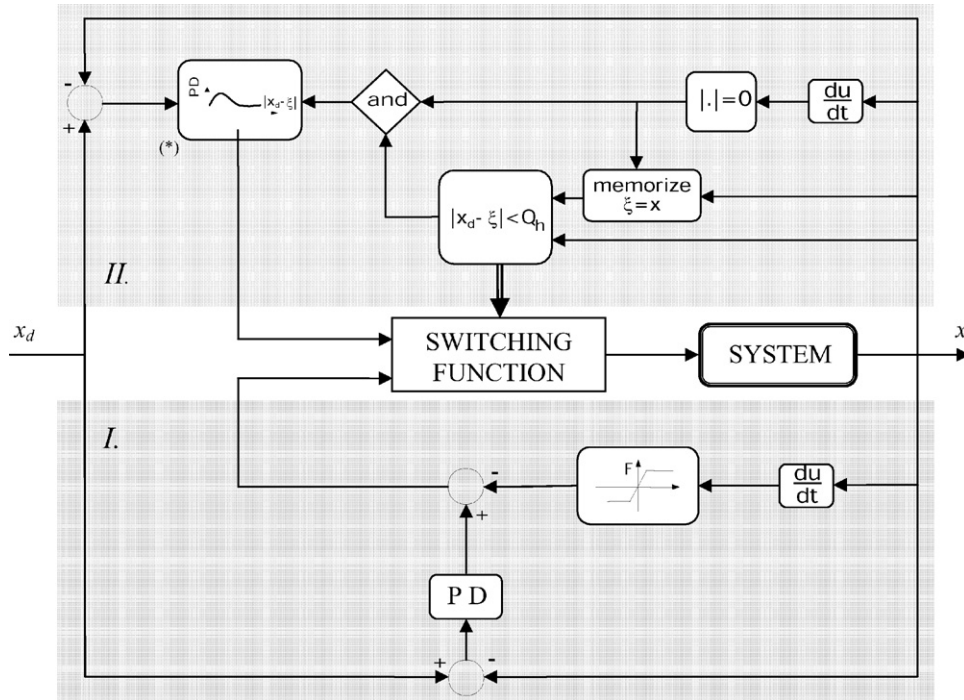


Fig. 10. The proposed gain scheduling controller scheme.

system subjected to the considered “hysteretic springs”, which can be modelled by the original Maxwell-slip model. They use a classical approach of the describing function [19] to obtain equivalent stiffness and damping of the system with hysteretic springs analytically. The equivalent dynamic parameters are then formulated as follows:

$$k_e = -\frac{4}{A\pi} \int_0^\pi y \left( \frac{A}{2} (1 - \cos(\theta)) \right) \cos(\theta) d\theta, \tag{5}$$

$$c_e \omega = -\frac{8}{\pi A^2} \int_0^A \left( y(\theta) - \frac{y(A)}{2} \right) d\theta, \tag{6}$$

where  $A$  is the amplitude of the motion and  $y(\theta)$  is the virgin curve of the hysteresis, which characterizes the behaviour of pre-sliding friction as a function of displacement,  $\theta$  (see Fig. 9), when relative motion takes place for the first time [18]. Based on the identified parameters from the previous section, the model of the virgin curve can be obtained. Utilizing Eqs. (5) and (6), the equivalent dynamic parameters as functions of amplitude of motion as described previously can then be calculated.

The controller consists of two different modes and it switches between those modes corresponding to the pre-sliding and the gross sliding regimes, respectively. The gain needs to be scheduled only in the first mode, i.e. within a certain stroke after motion reversal (see Fig. 10). A more comprehensive study on the gain scheduling controller for mechanical system with friction can be found in Refs. [20,21].

### 7. Compensation results of nonlinear controllers

In this section the performance of each controller will be presented considering two cases, namely a point-to-point (PTP) positioning system, as in a pick-and-place and spot-welding robot, and trajectory tracking system, such as used in a milling machine or a plotter.

In a PTP positioning system, a high accuracy and a short transition time are the most important performance criteria, while the path of the motion is less significant. Therefore, these requirements will become

the condition in designing the optimal performance of the controller in this paper. On the other hand, in a trajectory tracking case, performance of the controllers is quantified from the tracking error of the motion.

### 7.1. PTP positioning case

Fig. 11 shows a step response to 0.4 rad step input of the system with the proposed gain scheduling controller. The steady state error of the proposed gain scheduling controller resembles that of the classical cascade controller, they both lie below the resolution of the output encoder,  $10^{-4}$  rad error. However, the gain scheduling offers a significant advantage, since this controller does not contain an integrator part; it has a faster response. The dashed-line represents the response of the system when we used the first mode of the gain scheduling, which contains PD actions and Coulomb friction compensation, without switching to the second mode.

In the inset plot of Fig. 11 we can see the behaviour of the motion when the gains are adjusted after the velocity of the system reaches zero while the distance of the current position and the desired position is within the sticking limit (approximately 0.004 rad).

At the beginning, the first mode of the controller is active, which contains a linear PD controller with Coulomb friction compensation. When the motion reaches the steady position ( $v = 0$ ) at approximately 0.2 s (within a sticking distance to the desired position), the controller switches the second mode on and then the gains are re-adjusted based on the knowledge of the equivalent dynamic parameters. As a consequence, the control input will increase and the system will have an additional force. In turn, the system will move again approaching the desired position until it reaches another steady position and the gains will be adjusted repeatedly.

From the inset of Fig. 11, we can also see that at the beginning, the gain scheduling controller gives the same response time compared to the system with the DNPf controller. But when the motion gets closer to the desired position (within the pre-sliding distance to the desired position), the system with DNPf controller gives a faster response due to the continuous augmenting of the gain (the constant control input part in the DNPf, see Fig. 9), while the proposed controller increases the gain only after the velocity is equal to zero. However, the extra compensation force in the DNPf controller is not adequate to bring the motion to the desired position, since the additional force was designed based only on the static friction force of the system.

### 7.2. Trajectory tracking case

The DC motor system with the cascade controller and velocity feedforward is utilized for the trajectory tracking case. Based on the fact that the effect of pre-sliding regime dominates the friction in low-frequency motion as concluded from model-based feedforward compensation experiments, the study of the controllers

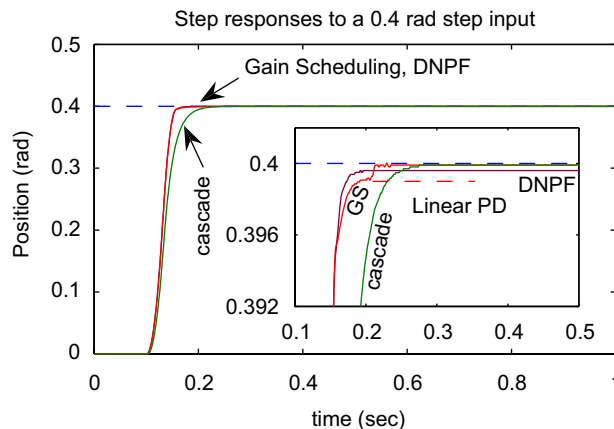


Fig. 11. Responses to 0.4 rad step input using various controllers.

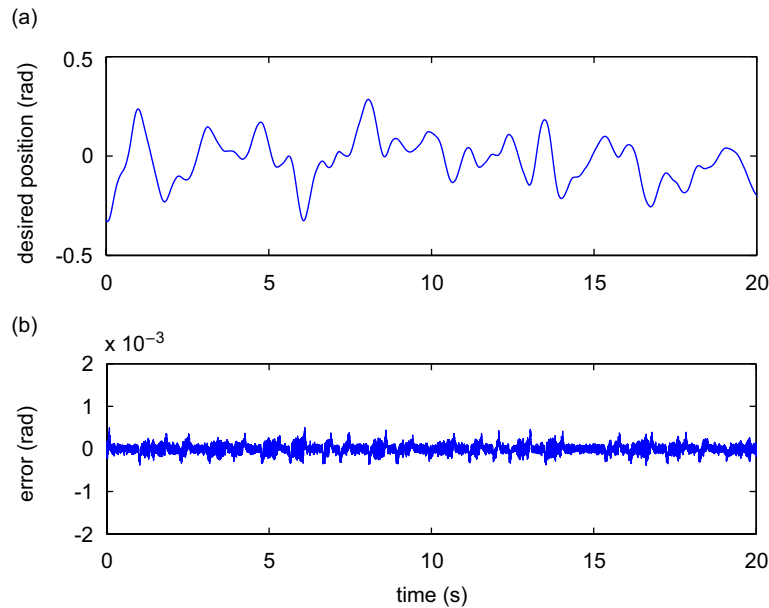


Fig. 12. The trajectory tracking performance for a system with cascade controller and velocity feedforward: (a) the reference position signal, (b) the tracking error.

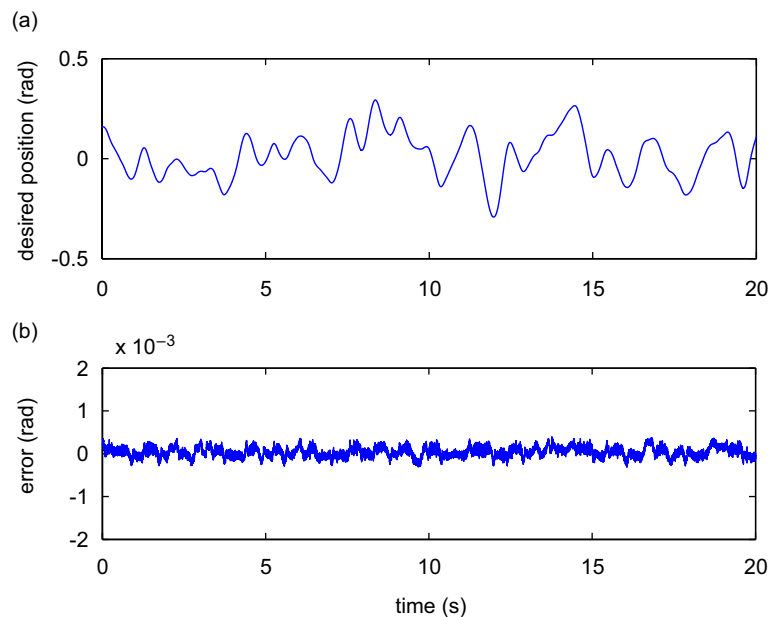


Fig. 13. The trajectory tracking performance for a system with DNPF controller: (a) the reference position signal, (b) the tracking error.

for trajectory tracking case will be implemented by imposing a random input with relatively low bandwidth frequency of 1 Hz on the system.

The upper panel of Fig. 12 shows the desired trajectory. The tracking error of this system can be seen in the lower panel of the same figure, where the root-mean-square of the error is equal to  $1.0 \times 10^{-4}$  (RMS) and the maximum error is approximately  $5.0 \times 10^{-4}$  rad.

As a second case, the system with the DNPF controller is implemented. An input signal with the same property as in the previous case is performed and the result is shown in Fig. 13. The upper panel depicts the

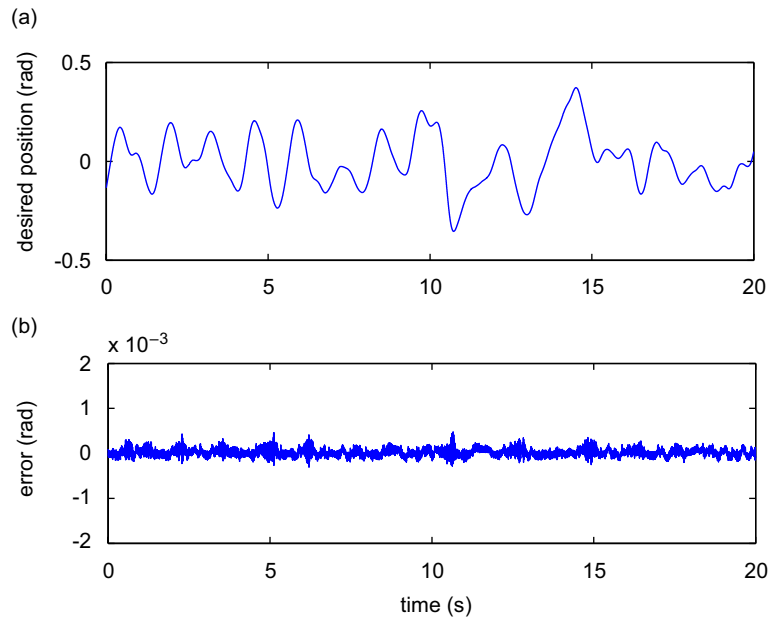


Fig. 14. The trajectory tracking performance for a system with gain scheduling controller: (a) the reference position signal, (b) the tracking error.

Table 4  
Performance of the controllers

Compensation	RMS ( $10^{-4}$ rad)	Max. error ( $10^{-4}$ rad)
Cascade	1.0	5.0
DNPF	1.1	4.1
Gain scheduling	0.8	4.8

input signal, while the lower one shows the tracking error. As quantification of the performance, the error is approximately equals to  $1.1 \times 10^{-4}$  RMS, while the maximum the error is approximately  $4.1 \times 10^{-4}$  rad.

As a final case, a gain scheduling controller, which has been discussed in Section 6, is implemented on the same system for trajectory tracking case. In order to have a fair comparison, a similar input to the system as in the previous cases is also used as can be seen in the upper panel of Fig. 14. The lower panel of Fig. 14 represents the tracking error of the system. Quantitatively, the controller exhibits a satisfactory result with  $0.8 \times 10^{-4}$  RMS and  $4.8 \times 10^{-4}$  rad maximum error. The performance quantifiers of each controller are tabulated in Table 4, where it is seen that there are no significantly large differences between them.

## 8. Conclusion

The following conclusions can be drawn from this investigation:

- Different friction model structures exist ranging in complexity from the Coulomb to the GMS model. Model-based friction identification using a single experiment is possible to achieve. However, selection of the excitation signal plays an important role for identification using single experiment.
- For motions with high displacement, the classical models such as Coulomb friction and the Stribeck friction model give satisfactory results that are comparable to the advanced models. However, at low displacements, which emphasize the pre-sliding regime, the classical models fail to give a satisfactory

estimation of the overall friction. For a good estimation in pre-sliding, models that incorporate hysteresis behaviour are necessary.

- The ability to estimate the friction behaviour in pre-sliding regime is the superiority of GMS model, while it does not lose its ability to estimate the friction in the sliding regime. Therefore the GMS model can capture friction behaviour for any working range of displacement and velocity.
- The nonlinear effect of friction in a high load torque DC motor is successfully compensated for in a feedforward based control experiment. In all of the validation cases, the GMS model yields the best results. This can be understood since this (most recent model) accommodates the hysteresis behaviour with non-local memory for the pre-sliding regime friction, while modelling the gross sliding also.
- However, feedback compensation is a more effective way than the feedforward controller. In particular, the dynamic parameters-based gain-scheduling controller offers a good combination of a fast response and low steady state error. The steady state error is similar to the system with cascade controller, while the response time is comparable to the one with the DMPF controller.

## References

- [1] J. Adams, S. Payandeh, Methods for low velocity friction compensation: Theory and experiments, *Journal of Robotic Systems* 13 (6) (1996) 391–404.
- [2] B. Armstrong-Hélouvry, P. Dupont, C. Canudas de Wit, A survey of models, analysis tools and compensation methods for the control of machines with friction, *Automatica* 30 (7) (1994) 1083–1138.
- [3] B. Armstrong-Hélouvry, *Control of Machines with Friction*, Kluwer Academic Publishers, Massachusetts, 1991.
- [4] T. Prajogo, Experimental Study of Pre-Rolling Friction for Motion-Reversal Error Compensation on Machine Tool Drive Systems, PhD Thesis, Department Werktuigkunde Katholieke Universiteit Leuven, Belgium, 1999.
- [5] J. Swevers, F. Al-Bender, C.G. Ganseman, T. Prajogo, An integrated friction model structure with improved presliding behavior for accurate friction compensation, *IEEE Transformation on Automatic Control* 45 (4) (2000) 675–686.
- [6] F. Al-Bender, V. Lampaert, J. Swevers, Modelling of dry sliding friction dynamics: from heuristic models to physically motivated models and back, *Chaos: An Interdisciplinary Journal of Nonlinear Science* 14 (2) (2004) 446–460.
- [7] C. Canudas de Wit, H. Olsson, K.J. Åström, P. Lischinsky, A new model for control of systems with friction, *IEEE Transformation on Automatic Control* 40 (3) (1995) 419–425.
- [8] F. Al-Bender, V. Lampaert, J. Swevers, The generalized maxwell-slip friction model: a novel model for friction simulation and compensation, *IEEE Transactions on Automatic Control* 50 (11) (2005) 1883–1887.
- [9] S.C. Southward, C.J. Radcliffe, C.R. Mac-Cluer, Robust nonlinear stick-slip friction compensation, *Journal of Dynamic Systems, Measurement and Control* 113 (1991) 639–644.
- [10] L. Cai, G. Song, A smooth robust nonlinear controller for robot manipulator with joint stick–slip friction, in: *Proceedings of IEEE International Conference on Robotics and Automation*, Atlanta, 1993, pp. 449–454.
- [11] Wahyudi, K. Sato, A. Shimokohbe, Robustness evaluation of three friction compensation methods for point-to-point (PTP) positioning systems, *Robotics and Autonomous Systems* 52 (2005) 247–256.
- [12] F. Al-Bender, W. Symens, Towards effective motion control of rolling element guideways, in: *Proceedings of Fifth Euromech Nonlinear Dynamics Conference*, Eindhoven, The Netherlands, 2005, pp. 1846–1858.
- [13] V. Lampaert, J. Swevers, F. Al-Bender, Modification of the leuven integrated model structure, *IEEE Transactions on Automatic Control* 47 (4) (2002) 683–687.
- [14] F. Al-Bender, V. Lampaert, J. Swevers, A generalized maxwell-slip friction model: a novel model for friction simulation and compensation, *IEEE Transactions on Automatic Control* 50 (11) (2005) 1883–1887.
- [15] W.D. Iwan, A distributed-element model for hysteresis and its steady-state dynamic response, *Journal of Applied Mechanics* 33 (4) (1966) 893–900.
- [16] P.E. Gill, W. Murray, M.H. Wright, *Practical Optimization*, Academic Press, London, 1981.
- [17] J.H. Mathews, K.D. Fink, *Numerical Methods Using Matlab*, Upper Saddle River, Prentice Hall, New Jersey, 1999.
- [18] F. Al-Bender, W. Symens, J. Swevers, H. Van Brussel, Theoretical analysis of the dynamic behavior of hysteresis elements in mechanical systems, *International Journal of Non-Linear Mechanics* 39 (2004) 1721–1735.
- [19] R.H. Macmillan, *Non-Linear Control System Analysis*, Pergamon Press, Oxford, 1962.
- [20] T. Tjahjowidodo, Characterization, Modelling and Control of Mechanical Systems Comprising Material and Geometrical Nonlinearities, PhD Thesis, Department Werktuigkunde Katholieke Universiteit Leuven, Belgium, 2006.
- [21] T. Tjahjowidodo, F. Al-Bender, W. Symens, H. Van Brussel, A gain scheduling controller for friction compensation, manuscript in preparation, 2007.